Neuron
Report

Pupil Fluctuations Track Fast Switching of Cortical States during Quiet Wakefulness

Jacob Reimer,[1,*] Emmanouil Froudarakis,[1] Cathryn R. Cadwell,[1] Dimitri Yatsenko,[1] George H. Denfield,[1] and Andreas S. Tolias[1,2,*]
[1]Department of Neuroscience, Baylor College of Medicine, Houston, TX 77030, USA
[2]Department of Computational and Applied Mathematics, Rice University, Houston, TX 77005, USA
*Correspondence: jreimer@cns.bcm.edu (J.R.), atolias@cns.bcm.edu (A.S.T.)
http://dx.doi.org/10.1016/j.neuron.2014.09.033

SUMMARY

Neural responses are modulated by brain state, which varies with arousal, attention, and behavior. In mice, running and whisking desynchronize the cortex and enhance sensory responses, but the quiescent periods between bouts of exploratory behaviors have not been well studied. We found that these periods of "quiet wakefulness" were characterized by state fluctuations on a timescale of 1–2 s. Small fluctuations in pupil diameter tracked these state transitions in multiple cortical areas. During dilation, the intracellular membrane potential was desynchronized, sensory responses were enhanced, and population activity was less correlated. In contrast, constriction was characterized by increased low-frequency oscillations and higher ensemble correlations. Specific subtypes of cortical interneurons were differentially activated during dilation and constriction, consistent with their participation in the observed state changes. Pupillometry has been used to index attention and mental effort in humans, but the intracellular dynamics and differences in population activity underlying this phenomenon were previously unknown.

INTRODUCTION

Responses to external stimuli are strongly modulated by the brain's internal dynamics, which are organized around characteristic states that vary with arousal, attention, and behavioral context (Harris and Thiele, 2011; Iriki et al., 1996; Kahneman, 1973; Lee and Dan, 2012). Across multiple species, more active states are associated with cortical desynchronization, a reduction in the amplitude of low-frequency oscillations measured in EEG, LFP, or intracellular recordings. For example, primate cortex is more desynchronized during attentive states (Gould et al., 2011; Grent-'t-Jong et al., 2011; Rohenkohl and Nobre, 2011) and in REM sleep compared to deeper sleep stages (Colten and Altevogt, 2006).

Nonprimate mammals also display a spectrum of cortical dynamics during waking periods, from more synchronized to more desynchronized states, and this internal variability modulates responses to external stimuli (Hei et al., 2014; Zhuang et al., 2014). Specifically, recent work in awake mice has revealed that the cortex is desynchronized during bouts of exploratory behavior, such as whisking (Crochet and Petersen, 2006; Poulet and Petersen, 2008) and running (Bennett et al., 2013; Niell and Stryker, 2010; Polack et al., 2013), compared to stationary periods. In mouse primary visual cortex (V1), this desynchronization is coupled with an enhancement of sensory responses (Fu et al., 2014; Froudarakis et al., 2014) and a reduction in detection thresholds (Bennett et al., 2013), and similar effects are seen in primary somatosensory cortex (area S1; Zagha et al., 2013).

Between bouts of activity, there are longer epochs of "quiet wakefulness," periods of behavioral quiescence that have not been well studied. While previous reports have emphasized the average increase in low-frequency synchronous activity during quiet wakefulness, we observed second-to-second state fluctuations during these periods in both V1 and S1. Fast state fluctuations during quiet wakefulness were closely tracked by changes in pupil diameter. During dilation, we found that the cortex was desynchronized and more responsive to external stimuli, compared to constriction, when low-frequency oscillations were enhanced and ensemble correlations were increased. (In this study we always use "dilation" and "constriction" to refer to active dilating and constricting, and not the state of being dilated or constricted.) Furthermore, vasoactive intestinal peptide-expressing (VIP+) GABAergic interneurons and somatostatin-expressing (SOM+) interneurons were differentially modulated during dilation and constriction. These interneuron subtypes have recently been shown to participate in a canonical local circuit essential for the enhancement of visual responses during running (Fu et al., 2014), and our results suggest that this mechanism may be recapitulated in the state fluctuations that occur during quiet wakefulness.

RESULTS

Exploratory Behaviors Are Accompanied by Cortical Desynchronization and Pupil Dilation

We performed whole-cell patch-clamp recordings of layer 2/3 cortical neurons in awake mice (n = 111 total neurons from 38 animals) while monitoring treadmill motion, whisking behavior, eye movements, and pupil diameter (Figures 1A and 1B). All analyses in Figures 1, 2, and 3 were of spontaneous recordings, in order to avoid any confounding effects of visual stimuli. Periods of running, whisking, and eye movements usually occurred

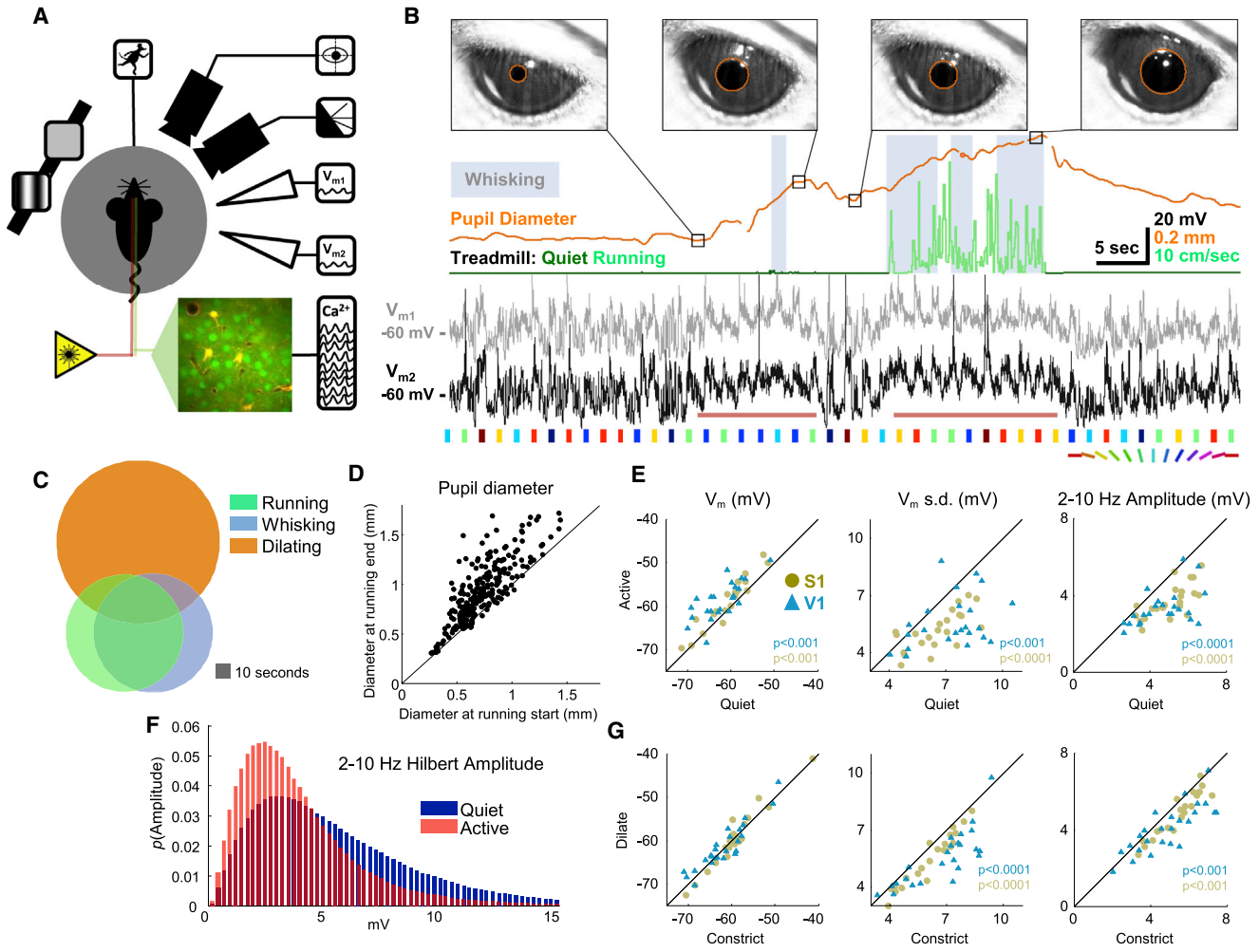

Figure 1. Pupil Diameter, Locomotion, and Whisking Correlate with Subthreshold Measures of Cortical State

(A) Schematic of simultaneous recordings showing mouse on spherical treadmill with eye and whisker cameras, single- or dual-patch pipettes, calcium imaging, and visual stimuli.

(B) Example treadmill activity (running periods in light green, see Supplemental Experimental Procedures), pupil diameter (orange), whisking (light blue background, see Supplemental Experimental Procedures), and V_m from two simultaneously patched cells (black and gray; depolarization around whisking and running epochs indicated with horizontal red lines). Colored patches below the voltage traces indicate presentations of oriented drifting gratings (Figure 4 only). Images of the eye are shown at the time points indicated in the pupil diameter trace, with pupil detection indicated by orange circles. Gaps in the pupil trace are due to blinks.

(C) Overlap of running, whisking, and pupil dilation episodes.

(D) Pupil size before and after running epochs.

(E) Changes in subthreshold membrane potential between quiet wakefulness and activity (running and whisking) without visual stimulation.

(F) Distribution of low-frequency amplitude during active behavior compared to quiet wakefulness.

(G) Changes in subthreshold membrane potential during dilating and constricting epochs of quiet wakefulness, also without visual stimuli. See also Figures S1 and S3 and Movie S1.

together (Figures 1C and S1; Movie S1), consistent with the idea that these behaviors are manifestations of a common exploratory state (Grant et al., 2012). Approximately 90% of these epochs were accompanied by an increase in pupil size (Figures 1B and 1D; mean increase in pupil diameter during running periods 202 ± 11 μm, mean ± SEM; see Experimental Procedures).

Consistent with previous studies (Bennett et al., 2013; Crochet and Petersen, 2006; Niell and Stryker, 2010; Polack et al., 2013; Poulet and Petersen, 2008; Zagha et al., 2013), we found that during exploratory behaviors (running and/or whisking), the membrane potential (V_m) in both S1 and V1 was desynchronized (red horizontal lines under example V1 recordings in Figure 1B). Relative to quiet wakefulness, V_m in these periods was depolarized (S1: 1.9 ± 0.4 mV, $p < 0.001$; V1: 3.6 ± 0.7 mV, $p < 0.001$) and less variable (change in V_m standard deviation, S1: −1.4 ± 0.2 mV, $p < 0.0001$; V1: −1.7 ± 0.4 mV, $p < 0.001$), and low-frequency oscillations were reduced (Hilbert amplitude of 2–10 Hz band-pass filtered V_m; S1: −1.4 ± 0.2 mV, $p < 0.0001$; V1: −1.3 ± 0.2 mV, $p < 0.0001$; Figure 1E; mean difference ± SEM; Wilcoxon signed-rank test for all comparisons). High-frequency

oscillations in the gamma range were also enhanced during activity compared to quiet wakefulness (Figure S1B), consistent with previous reports (Niell and Stryker, 2010).

During Quiet Epochs, Spontaneous Pupil Fluctuations Are a Sensitive Index of V_m Desynchronization

The large overlap in the amount of synchronous activity during active and quiet periods (Figure 1F) and the reliable increase in pupil size during the desynchronized periods associated with running and whisking led us to ask whether pupil dilation might also be associated with a desynchronized state during quiet wakefulness. To study quiet wakefulness, we excluded periods of running and whisking, and also saccades and blinks, which occurred rarely outside of active behaviors (less than one saccade per minute and less than one blink every 5 min; Figure S1A). We found that during quiet wakefulness, V_m variability was reduced during dilation versus constriction (change in V_m standard deviation, S1: -0.6 ± 0.08 mV, $p < 0.0001$; V1: -1.2 ± 0.2 mV, $p < 0.0001$). This effect could be explained primarily by a reduction in low-frequency oscillations (2–10 Hz Hilbert amplitude; S1: -0.56 ± 0.09 mV, $p < 0.001$; V1: -0.8 ± 0.2 mV, $p < 0.001$; Figure 1G; mean difference ± SEM; Wilcoxon signed-rank test for all comparisons). A modest increase in V_m oscillations at higher (gamma) frequencies was also observed during dilation compared to constriction (Figure S1C). However, in contrast with the effects of running and whisking, mean V_m was not significantly different for dilation versus constriction.

Pupil fluctuations were much smaller and faster during quiet wakefulness than around bouts of exploratory behavior (Figures 2A–2C; Movies S1 and S2). The duration of individual dilation and constriction periods during quiet wakefulness varied, although in general dilation was faster than constriction (mean dilating duration 1.6 s, mean constricting duration 2.0 s; Figure S2). In order to characterize the time course of the change in synchronous activity relative to pupil fluctuations during quiet wakefulness, we binned the instantaneous 2–10 Hz Hilbert amplitude by the phase of the pupil trace at each time point, aligning multiple cycles of dilation and constriction to one canonical cycle. We found that the amplitude of low-frequency V_m oscillations reached a minimum toward the middle of the dilating phase and peaked during constriction (Figure 2D; plots are mean ± SEM across cells). Overall, the average intracellular membrane potential was more desynchronized during dilation in both areas S1 and V1 (Figure 2E; S1 and V1, $p < 0.001$; paired t test; bars are mean change during dilation compared to constriction over cells, error bars are SEM; see also Figure S3). This relationship between cortical state and pupil fluctuations persisted even after removing occasional small postural adjustments or whisker twitches from our analysis and after habituating the mice to the treadmill for 30 min per day for 5 days prior to recording (Movie S1; Figure S4).

The robust link between pupil dilation and membrane potential desynchronization in area S1 argues against the possibility of a purely visual effect related to increased illumination of the retina. Although a small number of S1 cells (2/17) were weakly visually responsive (responsiveness generously defined as any significant change in V_m from baseline during a visual stimulus; $\alpha = 0.05$, Wilcoxon signed-rank test), the majority of visually unresponsive S1 cells still showed a robust relationship between dilation and V_m desynchronization (10/15; Figure 2F). To further rule out the possibility that changes in the visual input alone were responsible for cortical desynchronization, we patched cells in V1 of 8-week- to 4-month-old FVB/NJ (FVB) mice. In these mice, the retinal ganglion cell layer undergoes severe degeneration by P21 (Chang et al., 2002). In contrast to wild-type mice, where most of the V1 cells were visually responsive (12/13), none of the patched cells (0/9) were visually responsive in FVB mice. Yet the relationship between pupil fluctuations and cortical state was also observed in these cells (Figures 2D–2F; $p < 0.05$ Wilcoxon signed-rank test; Figure 2E). We did not observe a significant difference in the effect across the three groups of cells (S1, V1, FVB; one-way ANOVA, $p = 0.53$).

To examine whether state changes were tracked more closely by dilation and constriction or by pupil diameter, we examined the correlation between V_m synchronization and the derivative and absolute size of the pupil (Figures 2G and 2H). We found that the amplitude of 2–10 Hz oscillations was more closely tracked by the derivative than diameter of the pupil (mean fraction of variance explained in a two-way ANOVA for each cell by derivative, 0.13; by diameter, 0.05; $p < 0.0001$, t test).

A Local Interneuron Circuit Participates in the State Changes Tracked by Pupil Fluctuation

Recently, Fu and colleagues found that VIP+ interneurons are activated during running, while SOM+ interneurons are inhibited (Fu et al., 2014), consistent with several recent studies showing that VIP+ cells directly inhibit SOM+ cells, producing a net disinhibition of nearby pyramidal neurons. Furthermore, Fu et al. demonstrated that this cortical circuit was both necessary and sufficient to produce the enhancement of visual responses observed during running.

We initially sought to replicate the effect of active behavior on these interneuron subtypes with targeted patch recordings of labeled VIP+ ($n = 6$) and SOM+ ($n = 30$) cells in V1. Consistent with Fu et al., 2014, VIP+ cells were robustly depolarized during running (4.6 ± 0.8 mV; $p < 0.05$ Wilcoxon signed-rank test; Figures 3B and 3C). However, the behavior of SOM+ cells was more complex. We found that our SOM+ Cre driver line (SST-IRES-Cre; Taniguchi et al., 2011) labeled a population of neurons that could be grouped into two distinct classes, which we call Type I and Type II. Type I SOM+ cells, which were the majority ($n = 21/30$), exhibited the characteristic low V_m variability described by Petersen and colleagues (Gentet et al., 2012), and these cells were inhibited during active epochs of running and whisking (-2.1 ± 0.47 mV; $p < 0.001$ Wilcoxon signed-rank test; Figures 3A and 3C; Figure S5). A smaller population of Type II-labeled SOM+ cells ($n = 7/30$) had intrinsic membrane properties more similar to VIP+ or PV+ cells, and these cells were depolarized during active epochs (3.5 ± 0.9 mV; $p < 0.01$ Wilcoxon signed-rank test; Figure S5). In many cases, we recorded from both types of labeled SOM+ cells in the same animal, and they were completely separable by a number of features, the simplest being the range of voltages spanned by V_m during recordings of spontaneous activity (Figure S5). Both

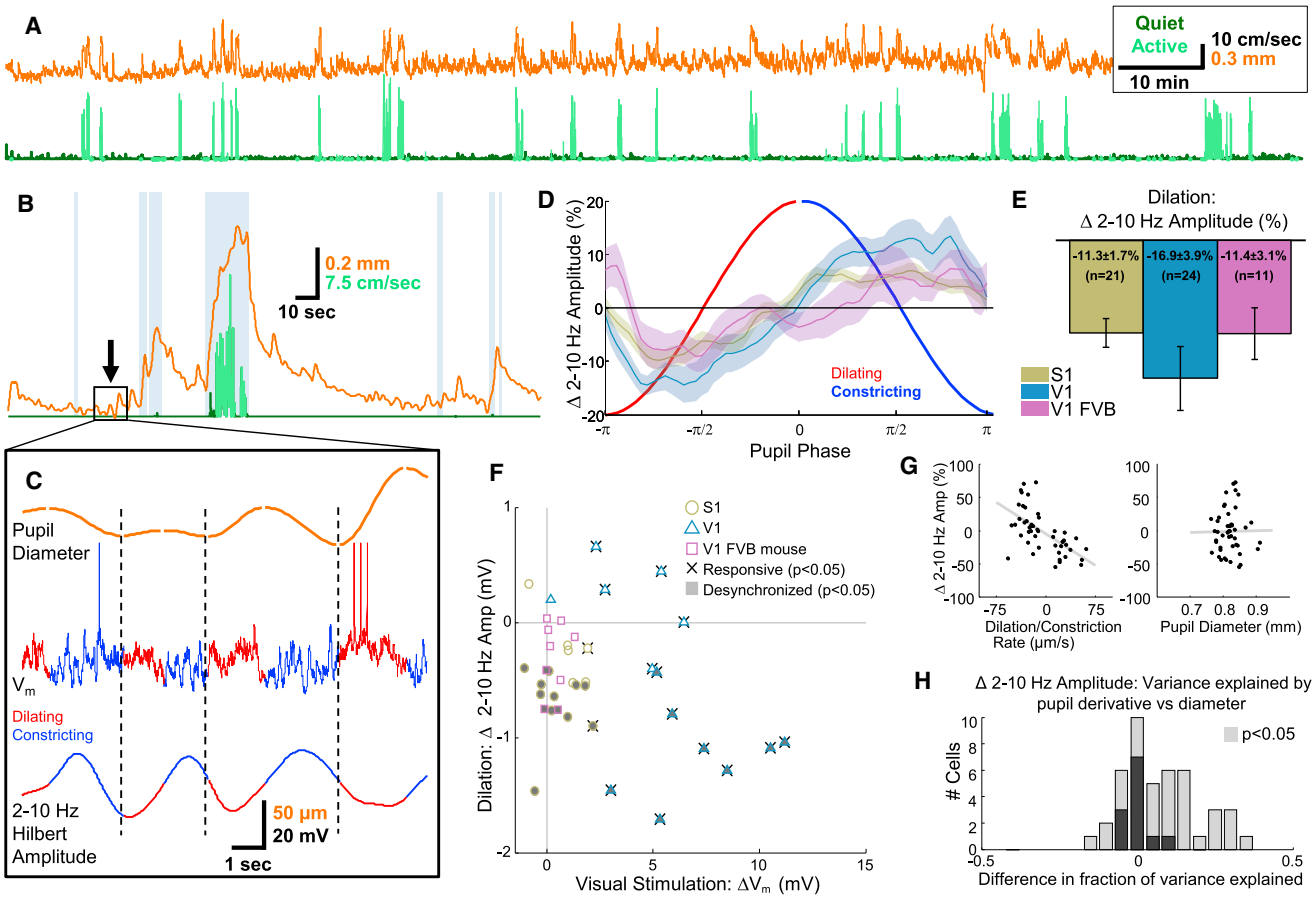

Figure 2. Pupil Diameter Correlates with Cortical State in the Absence of Exploratory Behavior

(A) Concatenated recordings of treadmill speed (running periods in light green, quiet periods in dark green) and pupil diameter (orange) from a single mouse (total time ~2.4 hr).

(B) Pupil diameter (orange) around a single active period (running in light green and whisking in light blue background).

(C) Zoomed-in period of quiet wakefulness from rectangle in (B) showing four sequential cycles of pupil dilation (red) and constriction (dark blue) correlated with low-frequency amplitude (separate cycles of dilation and constriction separated by dashed vertical lines).

(D) V_m is desynchronized during dilation and synchronized during constriction of the pupil in S1 (olive), V1 (blue), and V1 of FVB mice (mauve; 64 phase bins from $-\pi$ to π, plots are mean ± SEM for each bin).

(E) Averages over entire dilation and constriction periods for cells in each area (bar plots are mean ± SEM across cells, one-way ANOVA across cell groups was not significant $p = 0.53$).

(F) Scatterplot of desynchronization during dilation and visual responsiveness for all cells in each area. Significantly responsive cells are indicated with whiskers; significantly desynchronized cells are indicated with shading.

(G) Linear regression of the rate of change (left) and the absolute value of pupil diameter (right) against percent change in 2–10 Hz amplitude for a single cell.

(H) Stacked histogram of the difference in total variance in 2–10 Hz amplitude explained by pupil derivative and pupil diameter in a two-way ANOVA for each cell. Cells where either factor was significant ($p < 0.05$) are indicated with lighter bars. Overall, variations in cortical state indexed by low-frequency amplitude are more closely tracked by pupil dilation and constriction than by absolute pupil diameter ($p < 0.0001$, t test). See also Figures S2–S4 and Movie S2.

SOM+ Type I and Type II cells were distinct from morphologically identified (spiny) pyramidal cells, which were rarely labeled (n = 2/56), presumably due to leaky expression of Cre recombinase (Figure S5). Although the fact that the widely used SST-IRES-Cre line (Taniguchi et al., 2011) labels subpopulations of interneurons with different in vivo functional properties has not been previously reported, a recent in vitro study using these mice found two electrophysiologically distinct populations of labeled cells in almost the same proportions that we observed here (Hu et al., 2013). Based on these findings, we excluded Type II SOM+ cells in subsequent analyses.

Having confirmed the results of Fu et al. with respect to running, we wondered whether the SOM+/VIP+ cortical circuit might also participate in the state changes indexed by dilation and constriction during quiet wakefulness. Indeed, we found that VIP+ cells were relatively depolarized during dilation (2.1 ± 0.6 mV, $p < 0.05$) while SOM+ cells were hyperpolarized (−0.7 ± 0.3mV, $p < 0.05$; Wilcoxon signed-rank test for all comparisons; Figures 3D and 3E). Our results support the view that the SOM+/VIP+ circuit is not only recruited during active behavior, but may also play a role in cortical state changes during quiet wakefulness.

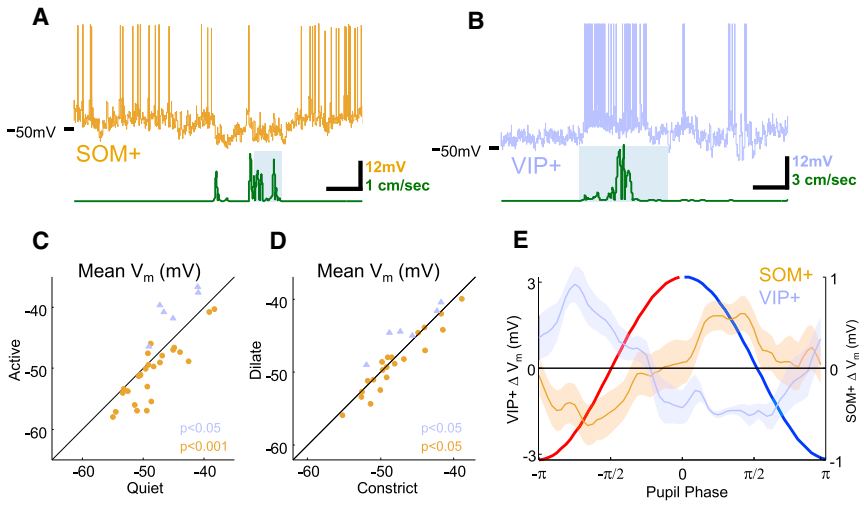

Figure 3. VIP+ Cells Are Excited and SOM+ Cells Are Inhibited during Active Behaviors and during Dilation

(A) Example SOM+ cell (brown) and treadmill (green) trace with whisking epoch as light blue rectangles in background. SOM+ cells are hyperpolarized during locomotion.

(B) Example VIP+ cell (blue) and treadmill (green) trace with whisking epoch as gray background. VIP+ activity is dramatically enhanced during running.

(C) Inhibition of SOM+ and excitation of VIP+ during exploratory behaviors compared to quiet wakefulness.

(D) In quiet wakefulness, SOM+ cells are inhibited and VIP+ cells are excited during dilation compared to constriction.

(E) Phase-binned change in SOM+ and VIP+ V_m showing time course of signature opposition of VIP+ and SOM+ activity over dilating and constricting periods (error bands are SEM).

Visual Encoding Is Improved during Desynchronized States Defined by Pupil Dilation

To determine whether stimulus encoding in V1 is improved during the desynchronized state indexed by pupil dilation, we performed two-photon calcium imaging of populations of layer 2/3 cells loaded with the calcium-sensitive fluorescent indicator Oregon Green BAPTA-1AM while presenting drifting oriented gratings (example site, Figures 4A and 4B; n = 34 imaging sites in six mice). We analyzed cells that were tuned for orientation (1,200/3,435 cells significantly tuned; see Experimental Procedures). During exploratory activity (running and whisking), there was a 20% increase in the mean response to preferred direction ($p < 10^{-12}$) and a 19% increase in the mean response to orthogonal directions ($p < 10^{-15}$; n = 516 tuned cells in 14 sites with sufficient numbers of visual responses during both active behavior and quiet wakefulness). These changes resulted in a slight decrease in orientation selectivity, but consistent with previous reports (Niell and Stryker, 2010; Polack et al., 2013), this change was not significant (7% decrease in OSI, p = 0.07; Figure 4C, error bands are SEM across cells). During quiet wakefulness, with running, whisking, and saccades removed, dilation was associated with a 9% increase in the mean response to preferred direction ($p < 10^{-13}$) and no change (0.6%, p = 0.47) in the response to the orthogonal direction, resulting in an enhancement of orientation selectivity (Figures 4D and 4E; 16% increase in OSI, $p < 10^{-6}$). Note that there was no significant difference in the size of the pupil between dilating and constricting trials (Figure S6). During dilation, responses to drifting gratings were also more reliable (Figure 4F; 28% increase in mean variability explained by stimulus conditions, $p < 10^{-15}$; n = 619 cells in 22 sites). Although there are a number of caveats that make it difficult to estimate the *absolute* magnitude of noise correlations using calcium imaging data (Cotton et al., 2013), we found that the relative magnitude of correlated activity varied significantly between the two states. There was a decrease in both signal and noise correlations during dilation versus constriction (Figures 4G and 4H; 20% decrease in mean noise correlations, $p < 0.0001$ and 16% decrease in mean signal correlations, $p < 0.01$; n = 21 sites, paired t test used for all comparisons; see Experimental Procedures). In summary, we found that responses to drifting gratings were more selective, more reliable, and less correlated during dilation compared to constriction.

We next asked whether visual encoding of natural stimuli was also enhanced during desynchronized states indexed by pupil dilation. We presented multiple repetitions of short prerecorded movies from a head-mounted camera of a mouse navigating an enriched environment. We performed calcium imaging in V1 (n = 53 imaging sites in seven mice). In addition to excluding running and whisking periods, we also removed saccades and any epochs where the eye deviated by more than 10° from its mean position. Correlating neural activity directly with changes in pupil size was not possible in this experiment because differences in brightness across frames elicited reliable dilations and constrictions of the pupil across multiple repetitions of the movie ($r = 0.61$ correlation of pupil size across trials for one example recording session, Figure 5A). To account for the effects of frame-to-frame changes in luminance, we sorted the responses to each 150 ms segment of the movie by the rate of change of pupil diameter and compared the neural responses for the upper and lower quartiles of the rates of change within each time bin (Figure 5B). Here, we assumed that the average change in pupil size over multiple movie repetitions (gray trace in Figure 5B) was due to luminance changes in the stimulus, while the variability around this average (blue and red vertical lines in Figure 5B) reflected the trial-to-trial differences in cortical state. Thus, for each bin, we compared "high" trials, when the pupil was dilating faster than usual (or constricting slower than usual) to "low" trials, when the pupil was dilating slower (or constricting faster) than the average.

Visual responses were enhanced during high trials compared to low trials (example cell in Figure 5C). Consistent with the increased OSI we observed for oriented gratings, responses to preferred frames of the movie were selectively enhanced during high trials compared to low trials (Figures 5D and 5E). Again, the pupil was not larger during high trials than low trials (Figure S6). At the population level, both signal (Figure 5F; $p < 0.001$) and

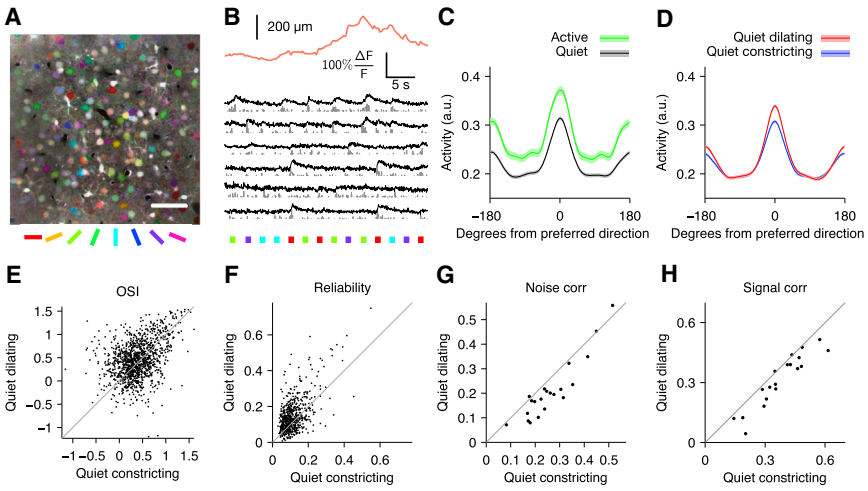

Figure 4. Orientation Tuning Is Enhanced during Pupil Dilation

(A) Mean fluorescence image colored by orientation preferences of individual pixels; scale bar, 50 μm.

(B) Example pupil diameter trace (orange) with simultaneous calcium traces from segmented cells (black) and inferred firing rates (gray). Colored squares indicate the direction of drifting gratings.

(C) Average tuning curves aligned to cells' preferred direction for active (running and/or whisking) periods (green) and quiet (black) periods. Peak responses are increased (20%, $p < 10^{-12}$) and orientation selectivity is unchanged (7% decrease, $p = 0.07$). Error bands are SEM computed over cells (n = 516).

(D) Average tuning during pupil dilation (red) and constriction (blue) during quiet periods (excluding running and whisking).

(E–H) Orientation selectivity is increased during dilation compared to constriction (16% increase in mean OSI, $p < 10^{-6}$) (E). Cells also respond more reliably during dilation compared to constriction (28% increase in mean binned R^2 values of stimulus responses of individual cells, $p < 10^{-15}$) (F). Across populations of neurons, mean noise correlations (G) ($p < 10^{-4}$) and signal correlations (H) ($p < 0.01$) are reduced during pupil dilation (n = 21 sites). Paired t test for all comparisons. Reliability and correlations are computed on 150 ms bins during stimulus presentations (see Supplemental Experimental Procedures).

noise (Figure 5G; $p < 0.05$) correlations were reduced, and there was an increase in the reliability (Figure 5H; $p < 0.001$) and discriminability (Figure 5I; $p < 0.001$) of responses during high trials compared to low trials (t test for all comparisons). In summary, consistent with the enhancement of responses to drifting gratings during dilation, responses to natural movies were more selective, more reliable, and less correlated during high trials.

DISCUSSION

We performed whole-cell patching and two-photon calcium imaging in awake mice (Bennett et al., 2013; Niell and Stryker, 2010; Polack et al., 2013) and focused our analysis on quiet periods between epochs of running and whisking. During these periods, we observed small spontaneous fluctuations in pupil diameter on a timescale of 1–2 s, which tracked changes in intracellular dynamics of L2/3 neurons in both somatosensory (S1) and visual (V1) cortex. V_m was desynchronized while the pupil was dilating and was dominated by low-frequency oscillations while the pupil was constricting. Dilation was accompanied by activation of VIP+ and inhibition of SOM+ interneurons, a phenomenon that has been shown to be essential to the enhanced visual responses observed during running (Fu et al., 2014). Using two-photon calcium imaging, we found that dilation was associated with an enhancement of visual responses and a reduction in both noise and signal correlations across ensembles of neurons for both gratings and natural stimuli.

For almost half a century, pupillometry has been widely used to index covert changes in attention and effort in humans and nonhuman primates (Gilzenrat et al., 2010; Hess and Polt, 1960, 1964; Iriki et al., 1996; Kahneman, 1973; Kahneman and Beatty, 1966; Kristjansson et al., 2009; Onorati et al., 2013; Wierda et al., 2012). Surprising and provocative stimuli produce a transient increase in pupil size (Bradley et al., 2008; Hess and Polt, 1960, 1964; Libby et al., 1973; Preuschoff et al., 2011), and pupil dilation preceding stimulus onset is correlated with faster reaction times in psychophysical tasks (Kristjansson et al., 2009). Our results provide evidence of changes in intracellular membrane potential dynamics and neural population activity underlying these psychophysical effects and emphasize the utility of pupil dilation and constriction as a proxy for noninvasively monitoring internal cortical states.

Previous authors have pointed out the analogy between desynchronization and enhanced sensory encoding during attention in primates, and the changes in cortical state during exploratory behaviors in mice (Harris and Thiele, 2011). Our results suggest that this analogy may be extended further, to encompass fluctuations in brain state in mice in the absence of overt behavioral changes. The ability to leverage mouse genetics to study the mechanisms that produce these state changes will be valuable, as will the ability to examine the potential dysregulation of brain state in mouse models of human disease.

Intracellular signatures of cortical activation were linked to pupil dilation across multiple cortical areas, suggesting that the effects we observe reflect a global change in brain state. Given the close relationship between pupil diameter, locus coeruleus activity, and sympathetic tone (Aston-Jones et al., 1999; Bradley et al., 2008; Gilzenrat et al., 2010), our data suggest a role for norepinephrine in the regulation of cortical state. Consistent with this notion, a recent study has implicated norepinephrine in the desynchronization that occurs during running (Polack et al., 2013). However, the potential contribution of other neuromodulators such as acetylcholine (Goard and Dan, 2009; Pinto et al., 2013) is also strongly suggested by the fact that the VIP+ activation during running has been shown to depend on cholinergic input from the diagonal band of Broca (Fu et al., 2014).

Additional mechanisms may also contribute to the state changes we describe here, which differ in at least two important ways from the state associated with exploratory behavior: First, unlike the effects of running, the desynchronization during

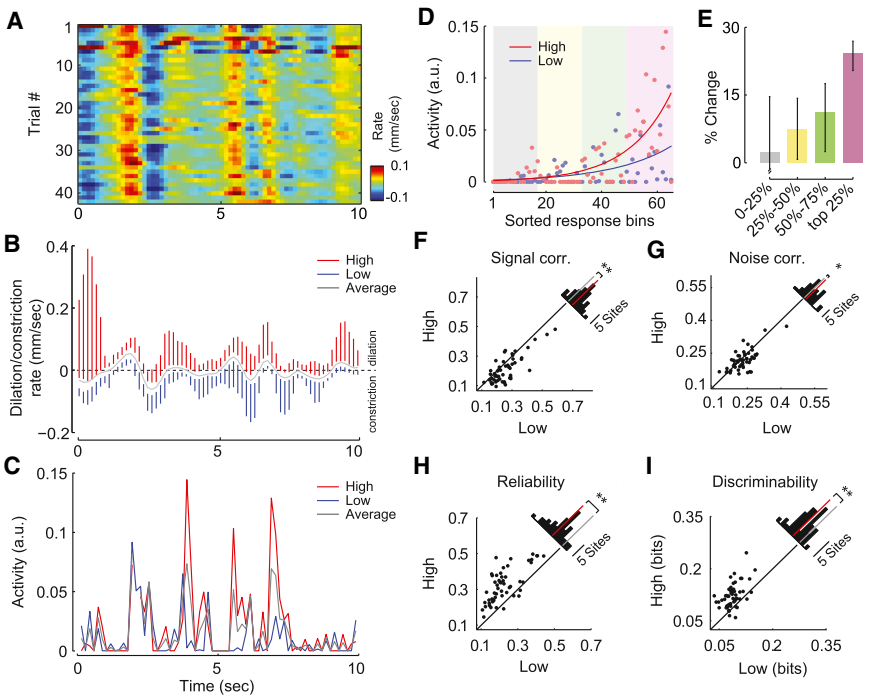

Figure 5. Encoding of Natural Images Is Improved during Pupil Dilation

(A) Pupil dilation/constriction rates across multiple repetitions of a natural movie.

(B) Mean (gray) and range in upper and lower quartiles (red and blue, respectively) of the pupil dilation/constriction rate for multiple presentations of a single movie (150 ms bins). Subsequent analyses compare neural responses in the upper quartile of pupil dilation/constriction rates ("high") to the lower quartile ("low").

(C) Increase in mean activity during high trials compared to low trials for a single cell.

(D) For each cell, movie frames are sorted by the mean neural response, not considering pupil dilation and constriction. Responses in high (red dots) and low (blue dots) conditions are fit with an exponential function (solid red and blue lines) to illustrate the selective increase in response to preferred stimuli.

(E) Median change in firing rate in high trials compared to low trials (n = 467 neurons, 95% confidence intervals) for least preferred (0%–25%), intermediate (25%–50% and 50%–75%), and most-preferred (75%–100%) frames for each cell. Responses to preferred frames are selectively enhanced.

(F–I) Mean signal (F) and noise (G) correlations decreased during the high condition, while reliability (H) and discriminability (I) were enhanced. Insets show histograms of absolute change with red bar indicating the mean difference (n = 53 sites, $^{**}p < 0.001$, $^{*}p < 0.05$, t test).

dilation is not accompanied by a significant depolarization of V_m. Second, we observe a qualitative difference in the effect of state on orientation tuning. During running, visual responses are enhanced at all orientations, while during dilation, responses at preferred orientations are enhanced without changing responses at orthogonal orientations, resulting in an increase in orientation selectivity. Further work will be necessary to uncover the mechanisms underlying these differences.

It is interesting to consider the potential computational role of continuous fluctuations in state during behaviorally quiescent periods. We speculate that during quiet wakefulness, the cortex may rapidly alternate between two distinct modes of information processing: a desynchronized state characterized by improved representation of feedforward sensory information and a synchronized state dominated by internally generated low-frequency network oscillations. Interestingly, theoretical work has suggested that alternating between bottom-up and top-down processing may be an efficient learning mechanism for the cortex to build a representation of the external world (Hinton, 2010).

EXPERIMENTAL PROCEDURES

All procedures were approved by the Institutional Animal Care and Use Committee (IACUC) of Baylor College of Medicine. Briefly, mice were anesthetized and a 3 mm craniotomy was made over the cortex as previously described (Froudarakis et al., 2014). For calcium imaging experiments, OGB1-AM was injected before sealing the craniotomy with a glass coverslip, which in some cases was prepared with a small (~500 μm) hole to allow pipette access. Following surgery, the mouse was placed on a treadmill with its head restrained beneath the microscope objective. Locomotion was detected by treadmill movement, and eye and whisker movements were detected optically. Whole-cell in vivo patching was performed using borosilicate patch pipettes (6–10 MΩ) filled with a standard low Cl^- internal solution (Jiang et al., 2013) as well as Alexa 488 or 598 for visualization. Visual stimuli were as follows: Figures 1, 2, and 3, blank screen; Figure 4, full-field square wave gratings (0.04 cycles/degree at 2 Hz, 500 ms trials interleaved with 1 s luminance-matched blanks, 100 repeats x 8 orientations); Figure 5, natural scene movies collected as previously described (Froudarakis et al., 2014). Calcium imaging was performed using either a standard galvo-galvo (Sutter Instruments) or resonant scanner (Thor Labs) using a Ti-Sapphire laser (Coherent) exciting at either 800 or 1,000 nm and equipped with either a 20× (1.0 NA, Olympus) or 25× (1.1 NA, Nikon) objective lens. Imaging data were motion-corrected and cell segmentation was manually supervised. A more detailed description of all experimental procedures can be found online in our Supplemental Experimental Procedures.

SUPPLEMENTAL INFORMATION

Supplemental Information includes Supplemental Experimental Procedures, six figures, and two movies and can be found with this article online at http://dx.doi.org/10.1016/j.neuron.2014.09.033.

AUTHOR CONTRIBUTIONS

J.R. collected and analyzed patching and calcium imaging data, performed pupil segmentation in all videos, and helped organize results and prepare the manuscript. E.F. helped build the behavioral apparatus and collected and analyzed calcium imaging data with natural movie stimuli. C.R.C. contributed to writing the paper and helped guide analyses. D.Y. created the DataJoint framework for data organization and analyzed calcium imaging data for oriented gratings. G.H.D. collected data and helped with manuscript revisions. A.S.T. supervised experiments, analysis, and preparation of the manuscript. E.F., C.R.C., and D.Y. contributed equally to this project.

ACKNOWLEDGMENTS

This work was supported by grants P30EY002520, T32EY07001, R01DA028525, DP1EY023176, and DP1OD008301 to A.S.T.; the McKnight

Scholar Award to A.S.T.; the Arnold & Beckman Foundation Young Investigator Award to A.S.T.; grants F30MH095440 and T32GM007330 to C.R.C.; and grant T32EB006350 to C.R.C. and D.Y. We thank Xiaolong Jiang for sharing his expertise in in vivo patching; Megan Rech, James Cotton, and Ryan Ash for helpful comments on the manuscript; and Ben Arenkiel for sharing the SST-IRES-Cre mouse line.

Accepted: September 22, 2014
Published: October 22, 2014

REFERENCES

Aston-Jones, G., Rajkowski, J., and Cohen, J. (1999). Role of locus coeruleus in attention and behavioral flexibility. Biol. Psychiatry *46*, 1309–1320.

Bennett, C., Arroyo, S., and Hestrin, S. (2013). Subthreshold mechanisms underlying state-dependent modulation of visual responses. Neuron *80*, 350–357.

Bradley, M.M., Miccoli, L., Escrig, M.A., and Lang, P.J. (2008). The pupil as a measure of emotional arousal and autonomic activation. Psychophysiology *45*, 602–607.

Chang, B., Hawes, N.L., Hurd, R.E., Davisson, M.T., Nusinowitz, S., and Heckenlively, J.R. (2002). Retinal degeneration mutants in the mouse. Vision Res. *42*, 517–525.

Colten, H.R., and Altevogt, B.M., eds. (2006). Sleep Disorders and Sleep Deprivation: An Unmet Public Health Problem (Washington, DC: National Academies Press).

Cotton, R.J., Froudarakis, E., Storer, P., Saggau, P., and Tolias, A.S. (2013). Three-dimensional mapping of microcircuit correlation structure. Front Neural Circuits *7*, 151.

Crochet, S., and Petersen, C.C.H. (2006). Correlating whisker behavior with membrane potential in barrel cortex of awake mice. Nat. Neurosci. *9*, 608–610.

Froudarakis, E., Berens, P., Ecker, A.S., Cotton, R.J., Sinz, F.H., Yatsenko, D., Saggau, P., Bethge, M., and Tolias, A.S. (2014). Population code in mouse V1 facilitates readout of natural scenes through increased sparseness. Nat. Neurosci. *17*, 851–857.

Fu, Y., Tucciarone, J.M., Espinosa, J.S., Sheng, N., Darcy, D.P., Nicoll, R.A., Huang, Z.J., and Stryker, M.P. (2014). A cortical circuit for gain control by behavioral state. Cell *156*, 1139–1152.

Gentet, L.J., Kremer, Y., Taniguchi, H., Huang, Z.J., Staiger, J.F., and Petersen, C.C.H. (2012). Unique functional properties of somatostatin-expressing GABAergic neurons in mouse barrel cortex. Nat. Neurosci. *15*, 607–612.

Gilzenrat, M.S., Nieuwenhuis, S., Jepma, M., and Cohen, J.D. (2010). Pupil diameter tracks changes in control state predicted by the adaptive gain theory of locus coeruleus function. Cogn. Affect. Behav. Neurosci. *10*, 252–269.

Goard, M., and Dan, Y. (2009). Basal forebrain activation enhances cortical coding of natural scenes. Nat. Neurosci. *12*, 1444–1449.

Gould, I.C., Rushworth, M.F., and Nobre, A.C. (2011). Indexing the graded allocation of visuospatial attention using anticipatory alpha oscillations. J. Neurophysiol. *105*, 1318–1326.

Grant, R.A., Mitchinson, B., and Prescott, T.J. (2012). The development of whisker control in rats in relation to locomotion. Dev. Psychobiol. *54*, 151–168.

Grent-'t-Jong, T., Boehler, C.N., Kenemans, J.L., and Woldorff, M.G. (2011). Differential functional roles of slow-wave and oscillatory-α activity in visual sensory cortex during anticipatory visual-spatial attention. Cereb. Cortex *21*, 2204–2216.

Harris, K.D., and Thiele, A. (2011). Cortical state and attention. Nat. Rev. Neurosci. *12*, 509–523.

Hei, X., Stoelzel, C.R., Zhuang, J., Bereshpolova, Y., Huff, J.M., Alonso, J.M., and Swadlow, H.A. (2014). Directional selective neurons in the awake LGN: response properties and modulation by brain state. J. Neurophysiol. *112*, 362–373.

Hess, E.H., and Polt, J.M. (1960). Pupil size as related to interest value of visual stimuli. Science *132*, 349–350.

Hess, E.H., and Polt, J.M. (1964). Pupil Size in Relation to Mental Activity during Simple Problem-Solving. Science *143*, 1190–1192.

Hinton, G.E. (2010). Learning to represent visual input. Philos. Trans. R. Soc. Lond. B Biol. Sci. *365*, 177–184.

Hu, H., Cavendish, J.Z., and Agmon, A. (2013). Not all that glitters is gold: off-target recombination in the somatostatin-IRES-Cre mouse line labels a subset of fast-spiking interneurons. Front Neural Circuits *7*, 195.

Iriki, A., Tanaka, M., and Iwamura, Y. (1996). Attention-induced neuronal activity in the monkey somatosensory cortex revealed by pupillometrics. Neurosci. Res. *25*, 173–181.

Jiang, X., Wang, G., Lee, A.J., Stornetta, R.L., and Zhu, J.J. (2013). The organization of two new cortical interneuronal circuits. Nat. Neurosci. *16*, 210–218.

Kahneman, D. (1973). Attention and Effort. (Englewood Cliffs, NJ: Prentice-Hall Inc.).

Kahneman, D., and Beatty, J. (1966). Pupil diameter and load on memory. Science *154*, 1583–1585.

Kristjansson, S.D., Stern, J.A., Brown, T.B., and Rohrbaugh, J.W. (2009). Detecting phasic lapses in alertness using pupillometric measures. Appl. Ergon. *40*, 978–986.

Lee, S.-H., and Dan, Y. (2012). Neuromodulation of brain states. Neuron *76*, 209–222.

Libby, W.L., Jr., Lacey, B.C., and Lacey, J.I. (1973). Pupillary and cardiac activity during visual attention. Psychophysiology *10*, 270–294.

Niell, C.M., and Stryker, M.P. (2010). Modulation of visual responses by behavioral state in mouse visual cortex. Neuron *65*, 472–479.

Onorati, F., Barbieri, R., Mauri, M., Russo, V., and Mainardi, L. (2013). Characterization of affective states by pupillary dynamics and autonomic correlates. Front Neuroeng *6*, 9.

Pinto, L., Goard, M.J., Estandian, D., Xu, M., Kwan, A.C., Lee, S.H., Harrison, T.C., Feng, G., and Dan, Y. (2013). Fast modulation of visual perception by basal forebrain cholinergic neurons. Nat. Neurosci. *16*, 1857–1863.

Polack, P.-O., Friedman, J., and Golshani, P. (2013). Cellular mechanisms of brain state-dependent gain modulation in visual cortex. Nat. Neurosci. *16*, 1331–1339.

Poulet, J.F.A., and Petersen, C.C.H. (2008). Internal brain state regulates membrane potential synchrony in barrel cortex of behaving mice. Nature *454*, 881–885.

Preuschoff, K., 't Hart, B.M., and Einhäuser, W. (2011). Pupil Dilation Signals Surprise: Evidence for Noradrenaline's Role in Decision Making. Front Neurosci *5*, 115.

Rohenkohl, G., and Nobre, A.C. (2011). α oscillations related to anticipatory attention follow temporal expectations. J. Neurosci. *31*, 14076–14084.

Taniguchi, H., He, M., Wu, P., Kim, S., Paik, R., Sugino, K., Kvitsiani, D., Fu, Y., Lu, J., Lin, Y., et al. (2011). A resource of Cre driver lines for genetic targeting of GABAergic neurons in cerebral cortex. Neuron *71*, 995–1013.

Wierda, S.M., van Rijn, H., Taatgen, N.A., and Martens, S. (2012). Pupil dilation deconvolution reveals the dynamics of attention at high temporal resolution. Proc. Natl. Acad. Sci. USA *109*, 8456–8460.

Zagha, E., Casale, A.E., Sachdev, R.N., McGinley, M.J., and McCormick, D.A. (2013). Motor cortex feedback influences sensory processing by modulating network state. Neuron *79*, 567–578.

Zhuang, J., Bereshpolova, Y., Stoelzel, C.R., Huff, J.M., Hei, X., Alonso, J.M., and Swadlow, H.A. (2014). Brain state effects on layer 4 of the awake visual cortex. J. Neurosci. *34*, 3888–3900.